A Reduced-order Observer-based LQR Control Method for Roll-to-roll Systems

Zhanpeng He, Zhihua Chen*, Xueqin Huang, Dong Ma

Institute of Computing Technology, Guangzhou University, China, Guangdong, Guangzhou, 510006
(Tel: +8613119536446; e-mail: 2112006102@e.gzhu.edu.cn; czhgd@gzhu.edu.cn;
2112006109@e.gzhu.edu.cn; 2112006033@e.gzhu.edu.cn).
** Corresponding Author: Zhihua Chen*

Abstract. Roll-to-roll (R2R) manufacturing is a flexible material manufacturing process with a high degree of automation and a low degree of cost. However, the complex characteristics make the high-precision register control a critical challenge. In this study, a reduced-order observer was designed to estimate the tension fluctuation value, and the estimated value was used to calculate the optimal control quantity through a linear quadratic regulator (LQR). Combined with the decoupling algorithm, a high-precision reduced-order observer-based LQR control (LQRC) is achieved. Simulations and comparisons confirmed that the register control method improves the control accuracy and adjustment time. Compared with the published fully decoupled proportional-derivative (FDPD) control algorithm, the control accuracy of LQRC was improved by at least 47%, and the adjustment time was reduced by at least 55%. Further, it was found that the LQRC method has a smoother control signal and consumes less energy compared with the FDPD control method. Overall, the results indicated that the LQRC method has good robustness and advantages in the practical application of industry.

Keywords: Roll-to-roll printing systems, Register control, Reduced-order observer, LQR control

1. INTRODUCTION

Roll-to-roll (R2R) manufacturing is widely used in the production of flexible materials because of its low manufacturing cost and high automation (Jung et al., 2014; Palavesam et al., 2018; Lee et al., 2019). The typical application of R2R manufacturing is the R2R printing machines (Figure 1 displays a schematic diagram of the R2R printing system used in the industry), and the key criterion is error registration accuracy (Abbel et al., 2018). The tension fluctuation of the printing material (also called web) leads to register errors, and it is induced by various factors such as disturbances and velocity changes. The R2R system is a complex coupling system with multi-inputs and multi-outputs. A high-precision register control is extremely important for R2R printing systems, but the control law is not trivial due to the complex coupling (Lee et al., 2020; Lee et al., 2020).

Fig. 1. A R2R printing system used in the industry.
Note. R2R: Roll-to-roll.

Some studies have been conducted on the register control of R2R systems. (Yoshida et al., 2008) and (Yoshida, 2008) deduced the register errors model and proposed a feedforward proportional derivative (PD) control method to eliminate the influence of the upstream control quantities on the downstream printing units, which improved the register accuracy of the R2R printing systems. Using new governing equations to minimize the effect of web tension on downstream printing units, (Torres and Pagilla, 2018) reduced the propagation of lateral perturbations. (Zhou et al., 2016) designed a control method for R2R systems for micro-contact printing to completely eliminate the coupling effect of the lateral motion of the web, achieving a precise control of ±200 nm. Likewise, (Nguyen et al., 2018) proposed a hyperbolic partial differential equation control method with two control inputs to reduce the lateral vibration of the web. Further, (Kim et al., 2020) designed an intelligent nonlinear tension and speed controller to improve the disturbance rejection performance and offset-free properties of R2R printing systems. (Zhang et al., 2021) proposed a direct-decoupling PD control method that completely eliminated the register errors caused by upstream control quantities. Moreover, a fully decoupled proportional-derivative control algorithm was proposed by (Chen et al., 2021) to completely eliminate the complex coupling relationship, thus improving the register accuracy.

The application of R2R systems in high-tech products poses higher requirements for register accuracy such as solar thin-film cells and flexible circuit boards (Dou et al., 2018; Gao et al., 2016; Bariya et al., 2018; Wang et al., 2021). Optimal control has rich theoretical support (Kim et al., 2010; Neilan et al., 2010) and is widely used in various industries (Buchholz et al., 2013; Zulkowski and DeWeese, 2015). In this study, a reduced-order observer-based linear quadratic regulator (LQR) optimal control method was proposed to estimate the tension fluctuation value. An LQR is designed according to the estimated tension fluctuation and measured register errors to calculate the optimal feedback control quantities. Experiments and comparisons indicated apparent improvement in the accuracy and adjustment time of the LQR control (LQRC) method proposed in the current study. This study is presented as follows:

In Section 2, a reduced-order observer is designed based on the mathematical model of R2R printing systems to estimate the tension fluctuation. In Section 3, an LQR optimal control is designed based on the estimated state variables. In Section 4, simulation and comparisons are carried to verify the effectiveness of the proposed LQR control algorithm. Finally, the conclusion is given in Section 5.

2. DESIGN OF REDUCED-ORDER OBSERVER

The simplified diagram of two adjacent printing units is illustrated in Figure 2. Each printing unit can print a mark that can run to the next printing unit as a reference. The registered error is defined as the position misalignment of the marks between the first and the current printing unit. Then, a mathematical model of printing registration can be derived based on the definition. The technological nomenclature used in this study is listed in Table 1.

Table 1. Nomenclature.

$\boldsymbol{r}$	Radius of gravure cylinder
$\boldsymbol{M}$	Elasticity coefficient
$\boldsymbol{\omega}^*$	Angular velocity of gravure cylinder at steady state
$\boldsymbol{T}^*$	Web tension at steady state
$\boldsymbol{l_i}$	Web length between *No.i* and *No.(i + 1)* gravure cylinder
$\boldsymbol{T_i(t)}$	Web tension between *No.i* and *No.(i + 1)* gravure cylinder at time *t*
$\boldsymbol{\omega_i(t)}$	Angular velocity of *No.i* gravure cylinder at time *t*
$\boldsymbol{E_i(t)}$	Register errors between *No.(i + 1)* and No.1 unit at time *t*
$\boldsymbol{\Delta T_i(t)}$	Tension fluctuation between *No.i* and *No.(i + 1)* gravure cylinder at time *t*
$\boldsymbol{\Delta\omega_i(t)}$	Variation of angular velocity of *No. i* gravure cylinder at time *t*

In Figure 2, T_i is the web tension which is the sum of ΔT_i and T^*, and ω_i denotes the angular velocity which is the sum of $\Delta\omega_i$ and ω^*. According to the law of conservation of mass, the relationship among the angular velocity of the gravure cylinder, the tension of the web, and the register errors, namely, the differential equation model of R2R printing systems, is as follows (Chen et al., 2021):

$$\begin{cases} \dfrac{d\Delta T_i(t)}{dt} = a_i\big(\Delta T_{i-1}(t) - \Delta T_i(t)\big) + \\ \qquad\qquad b_i\big(\Delta\omega_{i+1}(t) - \Delta\omega_i(t)\big) \\ \dfrac{dE_{i+1}(t)}{dt} = c\Delta T_i(t) \end{cases} \tag{1}$$

where $a_i = r\omega^* / l_i$, $b_i = r(1+MT^*)/Kl_i$, $c = Mr\omega^* / (1+MT^*)$.

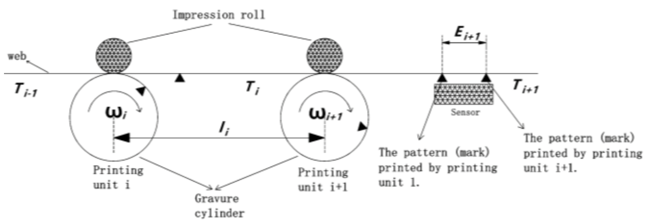

Fig. 2. The simplified diagram of the adjacent unit of R2R printing systems.
Note. R2R: Roll-to-roll.

From Eq. (1), it can be easily observed that the register error results from the tension change. To reduce the register errors, a state observer is designed to estimate the tension fluctuation value. The first thing to be done is to convert the mathematical differential model to a state space model.

Put *i=1* in Eq. (1), the *No.1* printing unit has no controller and is at a steady level with a steady speed, containing $\Delta\omega_1(t) = 0$, $\Delta T_0(t) = 0$, and $E_1(t) = 0$. Then, we have $x(t) = [\Delta T_1(t), E_2(t)]^T$, $u(t) = \Delta\omega_2(t)$, and $y(t) = E_2(t)$, so the state space model under this condition is:

$$\begin{cases} \begin{bmatrix} \Delta\dot{T}_1(t) \\ \dot{E}_2(t) \end{bmatrix} = \begin{bmatrix} -a_1 & 0 \\ c & 0 \end{bmatrix} \begin{bmatrix} \Delta T_1(t) \\ E_2(t) \end{bmatrix} + \begin{bmatrix} b_1 \\ 0 \end{bmatrix} \Delta\omega_2(t) \\ y(t) = \begin{bmatrix} 0 & 1 \end{bmatrix} \begin{bmatrix} \Delta T_1(t) \\ E_2(t) \end{bmatrix} \end{cases} \tag{2}$$

Put *i=1* and *i=2* in Eq. (1), then, we have $x(t) = [\Delta T_1(t), \Delta T_2(t), E_2(t), E_3(t)]^T$, $u(t) = [\Delta\omega_2(t), \Delta\omega_2(t)]^T$ and $y(t) = [E_2(t), E_3(t)]^T$, so the state space model under this condition is:

$$\begin{cases} \begin{bmatrix} \Delta\dot{T}_1(t) \\ \Delta\dot{T}_2(t) \\ \dot{E}_2(t) \\ \dot{E}_3(t) \end{bmatrix} = \begin{bmatrix} -a_1 & 0 & 0 & 0 \\ a_2 & -a_2 & 0 & 0 \\ c & 0 & 0 & 0 \\ 0 & c & 0 & 0 \end{bmatrix} \begin{bmatrix} \Delta T_1(t) \\ \Delta T_2(t) \\ E_2(t) \\ E_3(t) \end{bmatrix} \\ \qquad + \begin{bmatrix} b_1 & 0 \\ b_2 & -b_2 \\ 0 & 0 \\ 0 & 0 \end{bmatrix} \begin{bmatrix} \Delta\omega_2(t) \\ \Delta\omega_3(t) \end{bmatrix} \\ y(t) = \begin{bmatrix} 0 & 0 & 1 & 0 \\ 0 & 0 & 0 & 1 \end{bmatrix} \begin{bmatrix} \Delta T_1(t) \\ \Delta T_2(t) \\ E_2(t) \\ E_3(t) \end{bmatrix} \end{cases} \tag{3}$$

Accordingly, if we assume that the entire system has *n+1* printing units, put *i=1*, *i=2*, ⋯⋯, *i=n* in Eq. (1), then, the *2n×1* state vector can be defined as $x(t) = [\Delta T_1(t), \Delta T_2(t), \cdots\cdots, \Delta T_n(t), E_2(t), E_3(t), \cdots\cdots, E_{n+1}(t)]^T$, the *n×1* control vector is expressed as $u(t) = [\Delta\omega_2(t), \Delta\omega_3(t), \cdots\cdots, \Delta\omega_{n+1}(t)]^T$, and the *n×1* system output vector is defined as $y(t) = [E_2(t), E_3(t), \cdots\cdots, E_{n+1}(t)]^T$. The state space model of R2R printing systems can be obtained as follows:

$$\begin{cases} \dot{x}(t) = Ax(t) + Bu(t) \\ y(t) = Cx(t) \end{cases} \tag{4}$$

where $A = \begin{bmatrix} A_{11} & A_{12} \\ A_{21} & A_{22} \end{bmatrix}$, matrix A_{11}, A_{12}, A_{21} and A_{22} both are the square matrices of order *n*, $I(n)$ represents a unit matrix of order *n*, and $O(n)$ denotes a zero matrix of order *n*:

$$A_{11}=\begin{bmatrix}-a_1 & 0 & 0 & \cdots & 0 & 0\\ a_2 & -a_2 & 0 & \cdots & 0 & 0\\ 0 & a_3 & -a_3 & \cdots & 0 & 0\\ \vdots & \vdots & \vdots & \ddots & \vdots & \vdots\\ 0 & 0 & 0 & \cdots & -a_{n-1} & 0\\ 0 & 0 & 0 & \cdots & a_n & -a_n\end{bmatrix} \tag{5}$$

$A_{21}=c*I(n), A_{21}=A_{21}=O(n)$

and $B=[B_{11} \quad B_{21}]^T$, matrix B_{11} and B_{21} both are square matrices of order *n*:

$$B_{11}=\begin{bmatrix}b_1 & 0 & 0 & \cdots & 0 & 0\\ -b_2 & b_2 & 0 & \cdots & 0 & 0\\ 0 & -b_3 & b_3 & \cdots & 0 & 0\\ \vdots & \vdots & \vdots & \ddots & \vdots & \vdots\\ 0 & 0 & 0 & \cdots & b_{n-1} & 0\\ 0 & 0 & 0 & \cdots & -b_n & b_n\end{bmatrix}, \tag{6}$$

$B_{21}=O(n)$

and $C=[C_{11} \quad C_{21}]$, matrix C_{11} and C_{21} both are square matrices of order *n*:

$$C_{11}=O(n), C_{21}=I(n) \tag{7}$$

According to the Popov-Belevitch-Hautus observability criterion, when the inputs of R2R printing systems satisfy $u(t)=0$, the sufficient and necessary condition for the state vector $x(t)$ to be completely observable is that the matrix $[sI-A \quad C]^T$ is full rank, namely, rank $[sI-A \quad C]^T=2n$, where *s* is the eigenvalue of the state matrix *A*. As can be observed from Eq. (5), A is a *2n×2n* matrix, which has a total of *2n* eigenvalues, the *n* eigenvalues of matrix *A* are both zero, and the other *n* eigenvalues are $[a_1,a_2,\cdots,a_n]$, thus the rank of $(sI-A)$ is *n*. At the same time, it can be understood from Eq. (7) that the rank of the matrix C is also *n*. Therefore, the rank of $[sI-A \quad C]^T$ is *2n*, meeting the observability criterion, thus R2R printing systems have complete observability.

The output vectors are $[E_2(t),E_3(t),\cdots\cdots,E_{n+1}(t)]^T$, which are the last *n* state of the state vectors $x(t)$. Then, the *n* state vectors of R2R printing systems can be directly replaced by the *n* output vectors. It is necessary to establish an *n* dimensional reduced-order observer to reconstruct the remaining *n* state vectors.

Divide state vectors $x(t)=[\Delta T_1(t),\Delta T_2(t),\cdots\cdots,\Delta T_n(t), \Delta E_2(t),\Delta E_3(t),\cdots\cdots, \Delta E_{n+1}(t)]^T$ into $x_a(t)=[\Delta T_1(t), \Delta T_2(t),\cdots\cdots,\Delta T_n(t)]^T$ and $x_b(t)=[\Delta E_2(t),\Delta E_3(t),\cdots\cdots, \Delta E_{n+1}(t)]^T$. The state space model of R2R printing systems can be rewritten as:

$$\begin{cases}\begin{bmatrix}\dot{x_a}(t)\\ \dot{x_b}(t)\end{bmatrix}=\begin{bmatrix}A_{11} & A_{12}\\ A_{21} & A_{22}\end{bmatrix}\begin{bmatrix}x_a(t)\\ x_b(t)\end{bmatrix}+\begin{bmatrix}B_{11}\\ B_{21}\end{bmatrix}u(t)\\ y(t)=[C_{11} \quad C_{21}]\begin{bmatrix}x_a(t)\\ x_b(t)\end{bmatrix}=x_b(t)\end{cases} \tag{8}$$

Expand Eq. (8) to:

$$\begin{cases}\dot{x_a}(t)=A_{11}x_a(t)+A_{12}y(t)+B_{11}u(t)\\ \dot{y}(t)=A_{21}x_a(t)+A_{22}y(t)+B_{21}u(t)\end{cases} \tag{9}$$

define $z(t)=\dot{y}(t)-A_{22}y(t)-B_{21}u(t)$, then Eq. (9) can be derived as follows:

$$\begin{cases}\dot{x_a}(t)=A_{11}x_a(t)+A_{12}y(t)+B_{11}u(t)\\ z(t)=A_{21}x_a(t)\end{cases} \tag{10}$$

$A_{12}y(t)+B_{11}u(t)$ can be used as an input in Eq. (10), and $z(t)=\dot{y}(t)-A_{22}y(t)-B_{21}u(t)$ can be used as a known output in Eq. (10). A_{11} is the state matrix of the subsystem, and A_{21} is the output matrix of Eq. (10). Next, Eq. (10) is the deformation of Eq. (4), and its dimension is reduced, then a state observer can be established according to Eq. (10), and this observer is the reduce-order observer of Eq. (4) to estimate state vectors $x_a(t)$. According to the reduced-order observer design equation, we have:

$$\begin{cases}\dot{w}=(A_{11}-GA_{21})w+(B_{11}-GB_{21})u\\ \quad +[(A_{11}-GA_{21})G+A_{12}-GA_{22}]y\\ \quad =(A_{11}-GA_{21})(w+Gy)+B_{11}u\\ \hat{x}_a=w+Gy\end{cases} \tag{11}$$

where G is a $n\times n$ feedback matrix of the reduced-order observer, and the eigenvalues of the subsystem matrix $(A_{11}-GA_{21})$ can be arbitrarily configured through the pole configuration, while w is the intermediate variables to obtain the reconstructed state vector $\hat{x}_a(t)$. Combined with $x_b(t)=y(t)$, the estimate of the entire state vectors $\hat{x}(t)$ can be expressed as follows:

$$\hat{x}(t)=\begin{bmatrix}\hat{x}_a(t)\\ x_b(t)\end{bmatrix}=\begin{bmatrix}w(t)+Gy(t)\\ y(t)\end{bmatrix} \tag{12}$$

where $w(t)$, G, and $y(t)$ can be derived from Eq. (11), pole configuration, and detection sensor, respectively. Therefore, the state vector (tension fluctuation value) that cannot be measured can be estimated through these three known quantities.

According to Eqs. (11) and (12), the structure diagram of the reduced-order observer is illustrated in Figure 3.

Finally, the convergence of the reduced-order observer needs to be proved. Since the whole output vectors of the system can directly replace the half of state vectors, the error $e_a(t)$ between the real state vectors and the estimated state vectors of the remaining part is defined as:

$$e_a(t)=x_a(t)-\hat{x}_a(t) \tag{13}$$

Subsequently, taking the derivation of Eq. (13) and according to Eqs. (9), (11), and (12), we can obtain:

$$\begin{aligned}\dot{e_a}(t)&=\dot{x_a}(t)-\dot{\hat{x}_a}(t)\\ &=A_{11}x_a(t)+A_{12}y(t)+B_{11}u(t)-\dot{w}(t)-G\dot{y}(t)\\ &=A_{11}x_a(t)+A_{12}y(t)+B_{11}u(t)\dot{w}(t)\\ &\quad -[(A_{11}-GA_{21})(w+Gy)+B_{11}u]\\ &\quad -G[A_{21}x_a(t)+A_{22}y(t)+B_{21}u(t)]\\ &=A_{11}x_a(t)-(A_{11}-GA_{21})\hat{x}_a(t)-GA_{21}x_a(t)\\ &=(A_{11}-GA_{21})e_a(t)\end{aligned} \tag{14}$$

Eq. (14) indicates that $e_a(t)$ can converge to 0 as long as the matrix $(A_{11}-GA_{21})$ is configured as a negative diagonal matrix, suggesting that the gain matrix G of the reduced-order observer should be configured at a suitable position through the pole configuration. In this study, the main considerations are the rapid convergence of the tension estimation and the good poles. The pole configuration of the reduced-order observer in this paper is based on engineering practice.

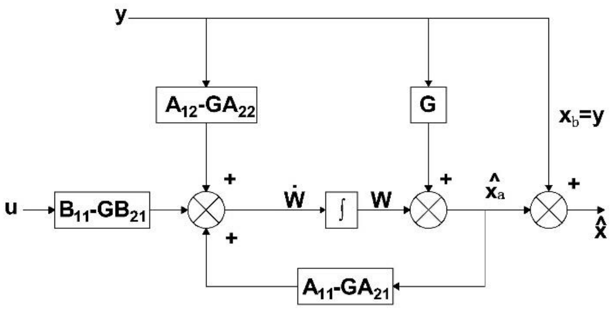

Fig. 3. The structure diagram of the reduced-order observer.

3. CONTROL METHOD

3.1 LQR control

Without considering the influence of coupling factors, each printing unit can be regarded as an independent individual, and the required control amount can be separately calculated. Initially, each printing unit of R2R printing systems is separately divided to calculate the basic control amount, and then the decoupling control amount is calculated according to the basic control amount. Finally, the total control amount of each printing unit is calculated, which consists of the basic optimal control amount and the decoupling control amount.

First, calculate the basic control amount of each printing unit. The state space equation and state feedback control law of arbitrary *No.i* printing unit can be written as:

$$\dot{\hat{x}}_i(t) = A_i\hat{x}_i(t) + B_i\Delta\omega_i(t) \tag{15}$$

$$\Delta\omega_i(t) = -K_i\hat{x}_i(t) = -K_{i1}\Delta\hat{T}_{i-1}(t) - K_{i2}E_i(t) \tag{16}$$

where $\hat{x}_i(t)$ is the state vector of *No.i* printing unit which is estimated by reduced-order observer, $\hat{x}_i(t) = \begin{bmatrix}\Delta\hat{T}_{i-1}(t)\\ E_i(t)\end{bmatrix}$, $A_i = \begin{bmatrix}-a_i & 0\\ c & 0\end{bmatrix}$, $B_i = \begin{bmatrix}b_i\\ 0\end{bmatrix}$, and $K_i = [K_{i1} \quad K_{i2}]$ is the state feedback gain matrix for *No.i* printing unit, while $\Delta\hat{T}_{i-1}(t)$ denotes the tension fluctuation estimated by the reduce-order observer.

The value of the state feedback gain matrix can be obtained by configuring the poles, but it is difficult to select the appropriate poles. Further, it is impossible to guarantee that the poles can achieve optimal control. Therefore, the state feedback control method in this study adopts the LQR to obtain the optimal control. It is necessary to set a performance function J_i and make this performance function a minimum value:

$$\begin{aligned} J_i = &\frac{1}{2}\hat{x}_i^T(t_{start})L_i\hat{x}_i(t_{start}) \\ &+\frac{1}{2}\int_{t_{start}}^{t_{end}}[\hat{x}_i^T(t)Q_i\hat{x}_i(t) + \Delta\omega_i^T(t)R_i\Delta\omega_i(t)]dt \end{aligned} \tag{17}$$

where L_i is a semi-positive definite terminal weighting matrix, Q_i is a semi-positive definite state weighting matrix, and R_i is a positive definite control weighting matrix. According to the minimum value principle, a 2-dimensional Lagrange multiplier vector $\lambda_i(t)$ is introduced to construct a Hamiltonian function to obtain the basic optimal control variable $\Delta\omega_i^*(t)$:

$$\begin{aligned} H_i[x,\Delta\omega,\lambda,t] = &\frac{1}{2}[\hat{x}_i^T(t)Q_i\hat{x}_i(t) + \Delta\omega_i^T(t)R_i\Delta\omega_i(t)] \\ &+\lambda_i^T(t)[A_ix_i(t) + B_i\Delta\omega_i(t)] \end{aligned} \tag{18}$$

Likewise, H_i should obtain an extreme value under optimal control. According to the method for finding the extreme value of the multivariate function, the partial derivative function of $\Delta\omega_i(t)$ is obtained by Eq. (18):

$$\frac{\partial H_i}{\partial\Delta\omega_i(t)} = R_i\Delta\omega_i(t) + B_i^T\lambda_i(t) \tag{19}$$

Let Eq. (19) be 0, since the matrix R_i is positive definite and symmetric, we have:

$$\Delta\omega_i^*(t) = -R_i^{-1}B_i^T\lambda_i(t) \tag{20}$$

and $\partial^2H_i/\partial[\Delta\omega_i(t)]^2 = R_i$, R_i is positive definite, thus Eq. (20) is the desired optimal control which causes performance function J_i to reach a minimum value.

The relationship between $\hat{x}_i(t)$ and $\lambda_i(t)$ can be solved by the canonical equation:

$$\dot{\lambda}_i(t) = -\frac{\partial H_i}{\partial\hat{x}_i} = -Q_i\hat{x}_i(t) - A_i^T\lambda_i(t) \tag{21}$$

The initial and equilibrium conditions are:

$$\begin{cases}\hat{x}_i(t_{start}) = x_0\\ \lambda_i(t_{end}) = \dfrac{\partial}{\partial x_i(t_{end})}\left[\dfrac{1}{2}x_i^T(t_{end})L_ix_i(t_{end})\right]\\ \qquad = L_ix_i(t_{end})\end{cases} \tag{22}$$

Eq. (21) can be solved according to the initial and equilibrium conditions as Eq. (22).

It is clear that $\Delta\omega_i^*(t)$ is a linear function of $\lambda_i(t)$ from Eq. (20). The transformation matrix $P_i(t)$ is a real symmetric positive definite matrix of 2×2-dimensional, then:

$$\lambda_i(t) = P_i(t)\hat{x}_i(t) \tag{23}$$

Substitute Eq. (23) into Eq. (20):

$$\begin{cases}\Delta\omega_i^*(t) = -K_i\hat{x}_i(t) = -R_i^{-1}B_i^TP_i(t)\hat{x}_i(t)\\ K_i = [K_{i1} \quad K_{i2}] = R_i^{-1}B_i^TP_i(t)\end{cases} \tag{24}$$

According to Eq. (24), the closed-loop system of *No.i* printing unit from Eq. (15) is:

$$\dot{\hat{x}}_i(t) = [A_i - B_iR_i^{-1}B_i^TP_i(t)]\hat{x}_i(t) \tag{25}$$

Eq. (25) implies that the optimal control can be realized by the optimal linear feedback composed of state vectors. Then the basic optimal control quantity of the state feedback is calculated below.

Substituting Eq. (23) into Eq. (21) and eliminating $\lambda_i(t)$, we can obtain:

$$\dot{\lambda}_i(t) = -Q_i(t)\hat{x}_i(t) - A_i^TP_i(t)\hat{x}_i(t) \tag{26}$$

At the same time, the derivation of Eq. (23) is as follows:

$$\dot{\lambda}_i(t) = \dot{P}_i(t)\hat{x}_i(t)+P_i(t)\dot{\hat{x}}_i(t) \tag{27}$$

By substituting Eqs. (25) and (26) into Eq. (27), we get:

$$\begin{aligned}&-Q_i(t)\hat{x}_i(t)-A_i^T P_i(t)\hat{x}_i(t)\\&= \dot{P}_i(t)\hat{x}_i(t) + P_i(t)[A_i - B_i R_i^{-1} B_i^T P_i(t)]\hat{x}_i(t)\end{aligned} \tag{28}$$

After arranging Eq. (28), the result is as follows:

$$\dot{P}_i(t) = -Q_i - A_i^T P_i(t) - P_i(t)A_i + P_i(t)B_i R_i^{-1} B_i^T P_i(t) \tag{29}$$

The value of the transformation matrix $P_i(t)$ can be obtained combined with condition $P_i(t_{end}) = L_i$. Finally, substituting $P_i(t)$ back into Eq. (24), the optimal control amount $\Delta\omega_i^*(t)$ and state feedback gain matrix K_i of *No.i* printing unit can be calculated. $\Delta\omega_i^*(t)$ is the basic optimal control quantity of *No.i* printing unit required in this subsection.

3.2 Decoupling control

Then, we should calculate the decoupling control amount according to the basic control amount in *3.1*. Since the upstream control quantities can induce the downstream register errors, it is necessary to eliminate the downstream register errors caused by the upstream control quantities. The decoupling compensation of *No.3* printing unit based on the model of Eq. (1) is as follows (Chen et al., 2021):

$$\begin{cases}\Delta\omega_3^{DC}(s) = \Delta\omega_{32}^{DC}(s) = F_2(s)\Delta\omega_2^*(s)\\ F_2(s) = \dfrac{s}{s+a_1}\end{cases} \tag{30}$$

Similarly, the decoupling compensation of *No.4* printing unit is as follows:

$$\begin{cases}\Delta\omega_4^{DC}(s) = \Delta\omega_{42}^{DC}(s) + \Delta\omega_{43}^{DC}(s)\\ \qquad\qquad = F_2(s)\Delta\omega_2^*(s) + F_3(s)\Delta\omega_3^*(s)\\ F_2(s) = \dfrac{s}{s+a_1}, F_3(s) = \dfrac{s}{s+a_2}\end{cases} \tag{31}$$

Accordingly, the decoupling compensation of *No.j* printing unit is as follows:

$$\begin{cases}\Delta\omega_j^{DC}(s) = \displaystyle\sum_{m=2}^{j-1} \Delta\omega_{jm}^{DC}(t), j \ge 3\\ \Delta\omega_{jm}^{DC}(t) = F_m(s)\Delta\omega_m^*(s), 2 \le m \le j-1\\ F_m(s) = \dfrac{s}{s+a_{m-1}}\end{cases} \tag{32}$$

where j represents any printing unit other than the *No.1* printing unit and the *No.2* printing unit, m represents the *No.m* printing unit before the *No.j* printing unit. $\Delta\omega_j^{DC}(s)$ represents the total decoupling control amount of *No.j* printing unit. And $\Delta\omega_{jm}^{DC}(s)$ represents the decoupling control amount for the *No.j* printing unit to eliminate the register errors caused by the register control amount of *No.m* printing unit. $\Delta\omega_m^*(s)$ is the optimal control quantity calculated based on the measured register errors of *No.m* printing unit. Then the calculation formula of a single optimal control quantity is:

$$\begin{cases}u_1^*(t) = 0, i = 1\\ u_2^*(t) = \Delta\omega_2^*(t), i = 2\\ u_i^*(t) = \Delta\omega_i^*(t) + \Delta\omega_i^{DC}(t), i > 2\end{cases} \tag{33}$$

If we assume that the entire system has *n+1* printing units, and defining total optimal control amount $u^*(t) = [u_2^*(t), u_3^*(t), \cdots\cdots, u_{n+1}^*(t)]^T$. According to Eqs. (32) and (33), the total optimal control amount $u^*(t)$ for all printing unit is:

$$u^*(t) = \begin{bmatrix}1 & 0 & 0 & \cdots & 0 & 0\\ F_2(t) & 1 & 0 & \cdots & 0 & 0\\ F_2(t) & F_3(t) & 1 & \cdots & 0 & 0\\ \vdots & \vdots & \vdots & \ddots & \vdots & \vdots\\ F_2(t) & F_3(t) & F_4(t) & \cdots & 1 & 0\\ F_2(t) & F_3(t) & F_4(t) & \cdots & F_n(t) & 1\end{bmatrix}\begin{bmatrix}\Delta\omega_2^*(t)\\ \Delta\omega_3^*(t)\\ \Delta\omega_4^*(t)\\ \vdots\\ \Delta\omega_n^*(t)\\ \Delta\omega_{n+1}^*(t)\end{bmatrix} \tag{34}$$

By combining the LQR control of *3.1* and the decoupling control of *3.2*, the structure diagram of the control method proposed in this study is illustrated in Figure 4.

Therefore, the state space model of R2R printing systems after decoupling can be written as:

$$\begin{cases}\dot{x}(t) = \begin{bmatrix}A_1^{DC} & A_2^{DC}\\ A_3^{DC} & A_4^{DC}\end{bmatrix}x(t) + \begin{bmatrix}B_1^{DC}\\ B_2^{DC}\end{bmatrix}u(t)\\ y(t) = [C_{11} \quad C_{12}]x(t)\end{cases} \tag{35}$$

where A_1^{DC}, A_2^{DC}, A_3^{DC}, A_4^{DC}, B_1^{DC} and B_2^{DC} both are square matrices of *n* order after decoupling control:

$$\begin{aligned}&A_1^{DC} = \begin{bmatrix}-a_1 & 0 & 0 & \cdots & 0 & 0\\ 0 & -a_2 & 0 & \cdots & 0 & 0\\ 0 & 0 & -a_3 & \cdots & 0 & 0\\ \vdots & \vdots & \vdots & \ddots & \vdots & \vdots\\ 0 & 0 & 0 & \cdots & -a_{n-1} & 0\\ 0 & 0 & 0 & \cdots & 0 & -a_n\end{bmatrix}\\ &A_2^{DC} = c * I(n), A_3^{DC} = A_4^{DC} = O(n),\\ &B_1^{DC} = \begin{bmatrix}b_1 & 0 & 0 & \cdots & 0 & 0\\ 0 & b_2 & 0 & \cdots & 0 & 0\\ 0 & 0 & b_3 & \cdots & 0 & 0\\ \vdots & \vdots & \vdots & \ddots & \vdots & \vdots\\ 0 & 0 & 0 & \cdots & b_{n-1} & 0\\ 0 & 0 & 0 & \cdots & 0 & b_n\end{bmatrix}, B_2^{DC} = 0\end{aligned} \tag{36}$$

$$u(t) = \begin{bmatrix}\Delta\omega_2^*(t)\\ \Delta\omega_3^*(t)\\ \Delta\omega_4^*(t)\\ \vdots\\ \Delta\omega_n^*(t)\\ \Delta\omega_{n+1}^*(t)\end{bmatrix} \tag{37}$$

It can be easily observed that Eq. (35) is a simple non-coupled multiple-input-multiple-output system after decoupling control, where $\Delta\omega_n^*(t)$ is the LQR control quantity of *No.i* printing unit designed based on the reduced-order tension observer.

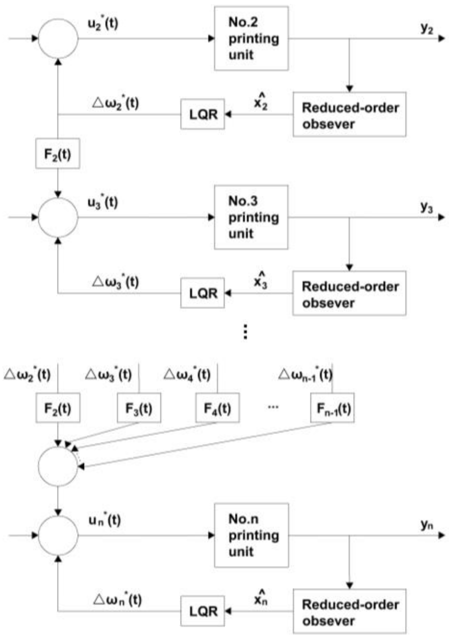

Fig. 4. Structure of the proposed control method.

4. INDUSTRIAL APPLICATION

The Eq. (1) has been validated by (Chen et al., 2021), thus it can be considered a real situation for R2R printing systems. In this study, a seven-printing unit electronic shaft gravure printing machine is used as an example to verify the effectiveness and superiority of the LQRC algorithm. Tables 2 and 3 present the system parameters and the poles of the designed reduced-order tension observer, respectively. The feedback gain matrix G of the reduced-order observer calculated from the configured poles is:

$$G = \begin{bmatrix} 4399.2 & 0 & 0 & 0 & 0 & 0 \\ 702.18 & 4026.4 & 0 & 0 & 0 & 0 \\ 0 & 702.18 & 3932.2 & 0 & 0 & 0 \\ 0 & 0 & 702.18 & 1269.8 & 0 & 0 \\ 0 & 0 & 0 & 702.18 & 1095.9 & 0 \\ 0 & 0 & 0 & 0 & 702.18 & 1682 \end{bmatrix}$$

Table 2. System parameters.

Parameters	Values
Printing speed	100 (m/min)
Web length l_i	6.48 (m)
Circumference of gravure cylinder r	0.53 (m)
Web tension at steady state T^*	100 (N)
Elasticity coefficient M	2.3×10^{-4} (1/N)

Table 3. The poles of reduced-order observer.

Unit	Pole
No.2 printing unit	-1.8686
No.3 printing unit	-1.7320
No.4 printing unit	-1.6975
No.5 printing unit	-0.7223
No.6 printing unit	-0.6586
No.7 printing unit	-0.8732

4.1 Closed-loop control

Given an initial disturbance with 3 mm to No. 2 printing unit, Figure 5 depicts the register errors of No. 2-7 printing units. It can be seen from Figure 5(a) that the register errors can be reduced to 0.1 mm after 42 sampling cycles and be kept at ±0.01 mm after 55 sampling cycles. The adjustment time is only 55 sampling cycles, and there is no excessive overshoot. Similarly, it can be observed from Figure 5(b) that the decoupling algorithm eliminates the register errors of downstream printing units caused by the control quantities of upstream printing units, and the register errors of No. 3-7 printing units can be kept at ±0.006 mm. The closed-loop register control of No. 2-7 printing units proves the effectiveness of the LQR control method.

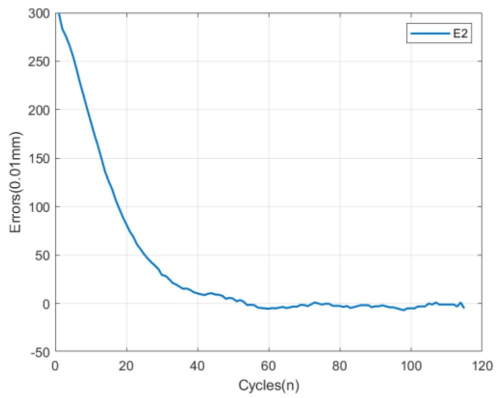

(a)

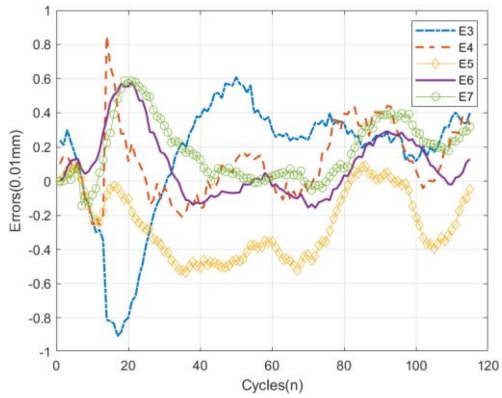

(b)

Fig. 5. Closed-loop register control errors of No. 2 printing unit to No. 7 printing unit.

4.2 Comparisons and analysis

Figure 6 presents the comparisons of the LQRC algorithm proposed in this study and the fully decoupled proportional-derivative (FDPD) algorithm. It can be seen from Figure 6(a) that the adjustment time of the No.2 printing unit of the LQRC algorithm and the FDPD algorithm is similar, but the LQRC algorithm has a smaller overshoot compared to the FDPD algorithm. Regarding the performance of the two algorithms in No. 3-5 printing units in Figure 6(b), the LQRC algorithm exhibits a 2-5 times improvement in register errors compared with the FDPD algorithm. In terms of adjustment time, the adjustment time of the LQRC algorithm is only 50% of that of the FDPD algorithm. As shown in Figure 6(c), the adjustment time of the LQRC algorithm on No. 6 and No. 7 printing units is only 30% of that of the FDPD algorithm.

It was shown that the violent change of control signal can exert a huge impact on the motor, serious bearing wear, and energy waste. The absolute values of each printing unit control for the LQRC and FDPD are summed up, respectively, and the results are shown in Figure 7. The sum of the absolute values of each printing unit control based on the FDPD method is kept at about 21 mm, while that of the LQRC method can be kept below 13 mm. The results reveal that the LQRC method is more stable and smoother compared to the FDPD method, which is more economical and applicable.

4.3 Anti-noise performance analysis

The bounded white noise module is used as the noise inputs to No. 2-4 printing units to analyze the anti-noise ability of LQRC. Figure 8 shows the comparisons of the register errors of No. 2-4 printing units with and without noise. It is evident from Figure 8(a) that the register errors of No. 2 printing unit also drop rapidly to the range of ±0.01 mm in the presence of noise, and the control curve is close to the curve without noise. Further, Figure 8(b) indicates that the register errors of No. 3 and No. 4 printing units can be controlled within ±0.006 mm with or without noise, and the control performances bear certain similarities. The results further indicate that LQRC method is robust for bounded noise disturbances.

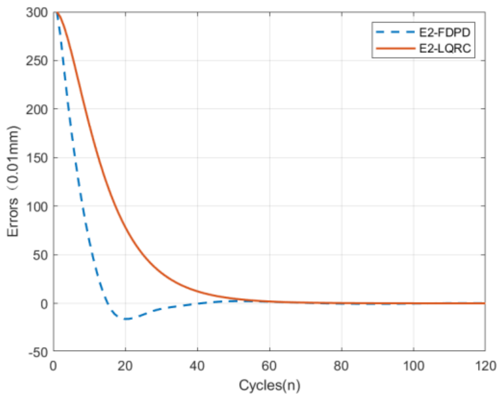

(a)

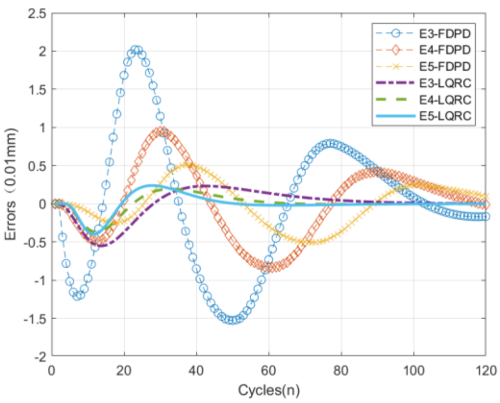

(b)

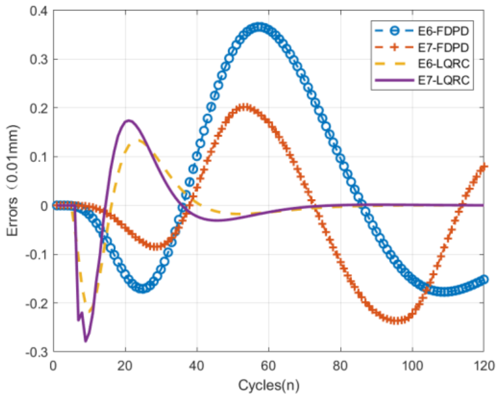

(c)

Fig. 6. Comparison of register error between LQRC and FDPD.

Note. LQRC: Linear quadratic regulator control; FDPD: Fully decoupled proportional-derivative

4.4 Parameter sensitivity analysis

The web length in Eq. (1) is a key system parameter and is obtained by manual measurement. Hence, there is inevitably a certain range of measurement noise. Therefore, it is necessary to verify the sensitivity of the LQRC algorithm to the key parameter. In this simulation, the web length of No. 5 and No. 6 printing units are both 6.48 m. The web length of No. 5 and No. 6 printing unit printing units change within the range of 86-118% and the range of 93-126%, respectively. Moreover, Figure 9 depicts the calculated register errors results using the LQRC algorithm. It can be found from Figure 9 that although the web length is not very accurate, the register errors of No. 5 and No. 6 printing units can be controlled within ±0.005 and ±0.0025 mm, respectively. Even if the web length has measurement errors, it will not affect the control effect of the LQRC, indicating that the LQRC has good fault tolerance and robustness for the measurement error of the web length.

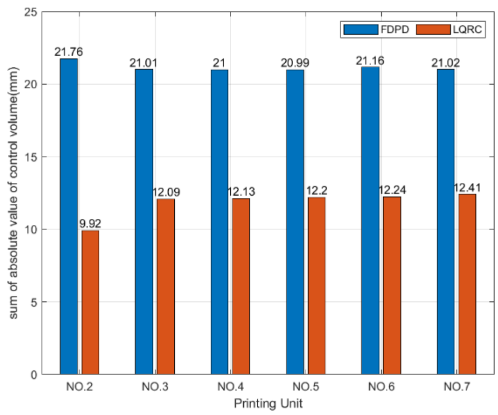

Fig. 7. Comparison of the sum of absolute value of the control value of each printing unit of FDPD and LQRC (mm).

Note. LQRC: Linear quadratic regulator control; FDPD: Fully decoupled proportional-derivative

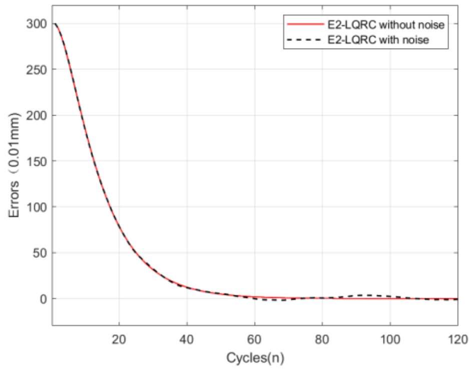

(a)

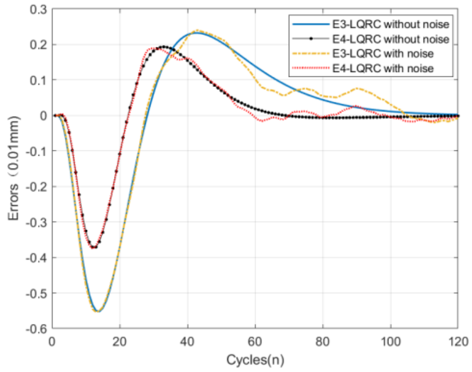

(b)

Fig. 8. Comparisons of register errors from No. 2 printing unit to No. 4 printing unit with and without noise.

Note. LQRC: Linear quadratic regulator control

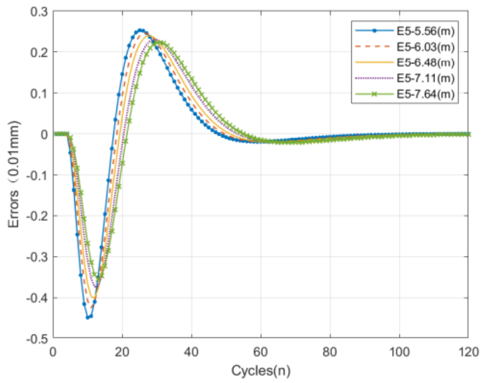

(a)

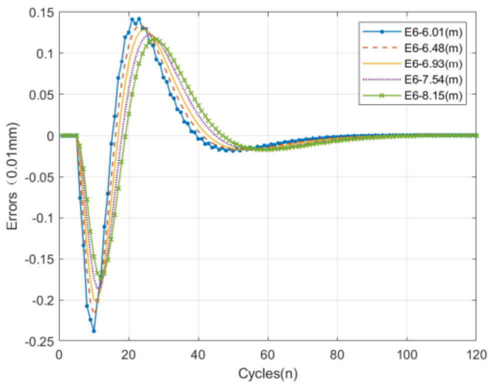

(b)

Fig. 9. Comparison of register error to No. 5 printing unit and No. 6 printing unit under inaccurate web length l_i.

5. CONCLUSIONS

In this study, a reduced-order observer-based LQRC is proposed. Compared with the newly published FDPD method, the LQRC method has the rapidity of the adjustment time, the stability of the control process, and the relative smoothness of control quantities. Further, the control accuracy of LQRC improves by at least 50% compared with that of the FDPD algorithm. At the same time, the sum of the absolute value of each printing unit control quantity is less than 60% of that of the FDPD, meaning that it not only impacts less wear and tear on the mechanical systems but also saves large energy for production process. The results further suggested that experiments and comparison experiments verify the control accuracy performance, anti-noise performance, and parameter sensitivity. The above analysis results showed that the LQRC method has good robustness and great advantages in the practical application of industry.

ACKNOWLEDGEMENTS

This work was supported by the National Natural Science Foundation of China (62272112), the Natural Science Foundation of Guangdong Province of China (2023A1515011998) and Science and Technology Projects in Guangzhou (202201020120).

The authors would like to express their gratitude to EditSprings (https://www.editsprings.cn) for the expert linguistic services provided.

REFERENCES

Abbel, R., Galagan, Y., and Groen, P. (2018). Roll-to-Roll Fabrication of Solution Processed Electronics. *Advanced Engineering Materials*, 20(8), 1701190.

Bariya, M., Shahpar, Z., Park, H., Sun, J., Jung, Y., Gao, W., ... & Javey, A. (2018). Roll-to-roll gravure printed electrochemical sensors for wearable and medical devices. *ACS nano, 12(7)*, 6978-6987.

Boscain, U., & Piccoli, B. (2005). An introduction to optimal control. *Contrôle non linéaire et applications,* Herman, Paris, 19-66.

Chen, Z., Zhang, T., Zheng, Y., Wong, D. S. H., & Deng, Z. (2021). Fully Decoupled Control of the Machine Directional Register in Roll-to-Roll Printing System. *IEEE Transactions on Industrial Electronics, 68(10),* 10007-10018.

Dou, B., Whitaker, J. B., Bruening, K., Moore, D. T., Wheeler, L. M., Ryter, J., ... & van Hest, M. F. (2018). Roll-to-roll printing of perovskite solar cells. *ACS Energy Letters, 3(10)*, 2558-2565.

Gao, Z., Bumgardner, C., Song, N., Zhang, Y., Li, J., & Li, X. (2016). Cotton-textile-enabled flexible self-sustaining power packs via roll-to-roll fabrication. *Nature communications, 7(1)*, 1-12.

Jung, M., Kim, J., Koo, H., Lee, W., Subramanian, V., & Cho, G. (2014). Roll-to-roll gravure with nanomaterials for printing smart packaging. *Journal of nanoscience and nanotechnology, 14(2)*, 1303-1317.

Kim, N., Cha, S., & Peng, H. (2010). Optimal control of hybrid electric vehicles based on Pontryagin's minimum principle. *IEEE Transactions on control systems technology, 19(5)*, 1279-1287.

Kim, S. K., & Ahn, C. K. (2020). Self-tuning nonlinear control system design for roll-to-roll printing systems. *IEEE/ASME Transactions on Mechatronics, 25(6),* 2667-2676.

Lee, B., Kim, Y., Kim, J., Park, J., Kim, H., & Oh, D. (2020). Preview control of web position in roll-to-roll printing using alignment patterns. *Microsystem Technologies, 26(11)*, 3315-3321.

Lee, J., Byeon, J., & Lee, C. (2020). Theories and control technologies for web handling in the roll-to-roll manufacturing process. *International Journal of Precision Engineering and Manufacturing-Green Technology, 7(2)*, 525-544.

Lee, J., Kim, S., & Lee, C. (2019). Surface drying for brittle material coating without crack defects in large-area roll-to-roll coating system. International Journal of *Precision Engineering and Manufacturing-Green Technology, 6(4)*, 723-730.

Marchetti, L., Priami, C., & Thanh, V. H. (2017). Simulation algorithms for computational systems biology. Berlin, Germany: *Springer International Publishing.*

Nguyen, Q. C., Piao, M., & Hong, K. S. (2018). Multivariable adaptive control of the rewinding process of a roll-to-roll system governed by hyperbolic partial differential equations. International Journal of Control, *Automation and Systems, 16(5)*, 2177-2186.

Palavesam, N., Marin, S., Hemmetzberger, D., Landesberger, C., Bock, K., & Kutter, C. (2018). Roll-to-roll processing of film substrates for hybrid integrated flexible electronics. *Flexible and Printed Electronics, 3(1)*, 014002.

Torres, E. O. C., & Pagilla, P. R. (2018, June). Modeling and Control of Web Lateral Dynamics in Roll-to-Roll Manufacturing: New Governing Equations and Control Strategies. I*n 2018 Annual American Control Conference (ACC)* (pp. 4452-4457). IEEE.

Wang, K., Wang, H., Zhou, X., & Yang, S. (2021, July). Working Parameter Optimization of a Microstructure Electrohydrodynamic Jet Printing System by the Quantification of Margins and Uncertainties. *In 2021 3rd International Conference on Intelligent Control, Measurement and Signal Processing and Intelligent Oil Field (ICMSP)* (pp. 134-140). IEEE.

Yoshida, T., Takagi, S., Muto, Y., & Shen, T. (2008). Modeling and resister control of sectional drive gravure printing press. *Transactions of the Japan Society of Mechanical Engineers, 74(742)*, 1438-1444.

Yoshida, T. (2008). Modeling and cooperative register control of gravure printing press. *Transactions of the Japan society of mechanical engineers C, 74(738)*, 339-345.

Zhang, T., Zheng, Y., Chen, Z., & Deng, Z. (2021). A Direct-Decoupling Closed-Loop Control Method for Roll-to-Roll Web Printing Systems. *IEEE Transactions on Automation Science and Engineering, 18(3)*, 1367-1379.

Zhou, X., Wang, D., Wang, J., & Chen, S. C. (2016). Precision design and control of a flexure-based roll-to-roll printing system. *Precision Engineering, 45*, 332-341.

Zulkowski, P. R., & DeWeese, M. R. (2015). Optimal control of overdamped systems. *Physical Review E, 92(3)*, 032117.